Journal of Materials Chemistry C

PAPER

View Article Online
View Journal | View Issue

Cite this: J. Mater. Chem. C, 2014, 2, 3744

Facile synthesis of phase-pure $FeCr_2Se_4$ and $FeCr_2S_4$ nanocrystals *via* a wet chemistry method†

Xiang Mao and Jaebeom Lee*

Received 11th December 2013
Accepted 14th February 2014

DOI: 10.1039/c3tc32453b

www.rsc.org/MaterialsC

We report a novel facile route for synthesis of iron-based ternary nanocrystals (NCs), *i.e.*, $FeCr_2Se_4$ and $FeCr_2S_4$, using a wet chemistry method. The electronic structure with a narrow band gap of Fe-based ternary semiconducting NCs with different dopants offers promising conductive properties. Owing significantly to the non-toxicity of their constituent materials, they exhibit higher potential for being utilized in solar cells than Cd and Pb-based compounds. The general route for synthesis of ternary compounds includes mixing and reacting of different elemental powders in evacuated silica ampoules for long periods of time under high temperature (700–1000 °C). However, this process results in an uncontrolled size and morphology of the colloidal NCs. In our proposed method, the NC morphology was easily controlled by the solvent and heating temperature, utilizing oleylamine as a surfactant, solvent, and reducing agent. The synthesized NCs possess excellent mono-dispersity of size and shape without any aggregation and the conductivities of the deposited layer of $FeCr_2Se_4$ and $FeCr_2S_4$ NCs are 3.25 μA and 2.33 μA, respectively. Therefore, these iron-based NCs may replace the use of chalcogenides that are known to be environmentally toxic, and may contribute to low efficiency of energy transfer.

Introduction

Metal chalcogenide materials have gained significant attention because of their interesting coordination, semiconducting behavior, and large binding affinity for metal ions.[1,2] Their applications range from bio-labeling to photocatalysis and photovoltaics that utilize either the discrete or collective properties of these size-controlled nanocrystals (NCs).[3] The synthesis of the archetypal binary (II–VI) NCs has progressed to where precise control over their size, shape, composition, and crystal phase has been achieved.[4,5] The extension of the colloidal NC synthesis method to ternary and quaternary semiconductors or other functional materials has great potential.[6–12] Metal-based ternary NCs such as MCr_2X_4 (where M = Cd, Zn, Hg and Co; X = S, Se, and Te) have been considered as functional materials and their structural analysis has been carried out.[13] The advancement in the colloidal synthesis and shape control of these bimetallic, ternary, and quaternary NCs has been demonstrated well enough, although copper composites remain elusive.[14–16]

Iron-based metallic NCs are mainly synthesized with the polyphase forms of FeSe, $FeSe_2$, $FeCr_2S_4$, $FeCr_2Se_4$, $Fe_{0.5}Cu_{0.5}Cr2Se_4$ and so on. These NCs are of interest because of abundant Fe and Cr resources, their unique superconducting and optical properties, and appropriate optical energy band gaps for solar cell application.[17–20] The synthesis and utilization of these materials are growing fields of research.[20,21] However, only a few studies have been reported on the synthesis of iron-based ternary materials using wet chemical synthesis methods.[21,22]

The Goldschmidt–Penn–Parrott law for crystal conductivity depicts $\Delta W/W \propto L_s^{1/2}$, where ΔW is the increase in crystal resistivity W and L_s indicates the average grain size.[23] This implies that the grain size of the crystals is an essential factor to be considered. Concurrently, crystal group contribution (λ_L) also influences the natural conductivity of the crystals: $\lambda_L = L\sigma T$, where L is the Lorentz factor, σ indicates the extent of the crystallization of the NCs and T is the temperature used for conductivity measurements. From these two equations, it can be concluded that for higher conductivity, smaller size and higher crystallinity are required.[24–26] Additionally, iron-based ternary NCs ($FeCr_2Se_4$ and $FeCr_2S_4$ NCs) are attractive for their electrical applications since their conductivities can be influenced by the external temperature and lattice contribution of the NCs as well as by the different dopants during synthesis.[27]

Recently, some studies have shown synthesis of $FeCr_2Se_4$ and $FeCr_2S_4$ NCs involving the use of powder precursors, hot-pressing, high-temperature (700–1000 °C), and additives leading to significant increases in the conductivity of the microscale products; however the synthesis is disadvantageous because of the scarcity and high cost of the metal precursors. Extensive efforts have been undertaken to develop highly

Department of Nano Fusion Engineering and Cogno-Mechatronics Engineering, Pusan National University, Busan, 609-735, Republic of Korea. E-mail: jaebeom@pusan.ac.kr

† Electronic supplementary information (ESI) available: Detailed experimental procedures, additional TEM and SEM images, EDX spectra, TGA, *I–V* curves, SQUID curves, and the image of fabrication devices. See DOI: 10.1039/c3tc32453b

conductive, durable, and low-cost alternative methods such as diffusion of metal transition elements[28] and high-temperature sealed methods.[29,30] However, most non-precious metal conductors suffer from poor conductivity. In addition, the facile synthesis of iron-based ternary metal chalcogenides with morphology control was not found to be practicable *via* wet chemistry methods.

Herein, we describe a novel wet chemistry method to synthesize colloidal crystals of mono-dispersed and phase-pure stoichiometric $FeCr_2Se_4$ and $FeCr_2S_4$ NCs with high yield. The synthesis method reported in this study is advantageous as it utilizes less energy, takes place under atmospheric pressure, and employs standard chemicals (Fe/Cr/Se/S composition, purity 98%). Moreover, the morphology control of the NCs was realized by the simple presence of a primary amine of alkene *i.e.*, oleylamine (OLA), due to solvent coordination and its passivation to the NC surface,[16b] which suggests that OLA can not only be used as the solution medium, but also as the stabilizer on the surface of the NCs in the passivation process. The reaction finished completely within 30 min. The anisotropic growth mechanism for NCs in a solid solution has been investigated in detail by controlling their growth kinetics, where the reaction temperature is an essential factor. At 330–360 °C, the formation of the NCs was predominantly favored, whereas below this range, only the precursors such as Cr_2S_3, Cr_3S_4, FeS, FeSe, or $FeSe_2$ were fabricated.[13c,31] Moreover, the electrical properties of the multi-layered NCs on a glass substrate with gold electrodes were demonstrated, offering the possibility of an optimum crystal structure *via* this synthesis method for efficient conductive devices. The magnetic properties of the NCs were also characterized.

Experimental details

Chemicals

Iron(II) acetylacetonate ($Fe(acac)_2$ 99.8%), chromium(III) acetylacetonate ($Cr(acac)_3$, 99.8%), anhydrous acetonitrile (>95%), 1,2-ethanedithiol (EDT, 95%), selenium powder (100 mesh, 98%), oleylamine (OLA, 98%), 1-dodecanethiol (1-DDT, 98%), toluene (99%), chloroform (99%), isopropanol (90%), and ethanol (90%) were used. All of these chemicals were purchased from Sigma-Aldrich.

Selenium precursor preparation

10 mL of OLA and 0.03 mol of Se powder were mixed in a flask and vacuum-pumped at 120 °C for 30 min. Subsequently, the flask was purged with N_2 during the reaction to prevent any unwanted oxidation. This solution was heated at 330 °C for over 1 h and maintained at that temperature for an hour. When the Se powder completely dissolved in OLA, the color of the solution changed from colorless to maroon, finally attaining a faint yellow hue.

Synthesis of $FeCr_2Se_4$ NCs

$FeCr_2Se_4$ NCs were synthesized under N_2 without any water and in the presence of oxygen using standard Schlenk techniques. A typical synthesis of $FeCr_2Se_4$ NCs is detailed as follows; first, 0.025 mmol $Fe(acac)_2$, 0.50 mmol $Cr(acac)_3$ and 10 mL OLA were mixed at room temperature, where the molar ratio of Fe : Cr was carefully investigated to optimize for a homogeneous product (see Fig. S5† for further details). The mixed solution was cycled between vacuum and N_2 three times. Afterwards, the mixture was kept at 60 °C under vacuum for 1 h, and then heated to 120 °C under vigorous stirring. 10 min later, the mixture was heated directly to 335 °C. Once the temperature reached 335 °C, 1 mL of the prepared Se precursor was dropped into the mixture at an injection rate of 3 drops per second using a 10 mL injection syringe under vigorous stirring. The temperature was kept at 335 °C for another 30 min after completion of the injection. Then, the flask was cooled to room temperature to produce the NCs.

The synthesized NCs were purified by precipitation with isopropanol *via* centrifugation at 8500 rpm for 20 min and re-dispersed in toluene or chloroform. After repetition of the washing step for 3–4 times, the supernatant containing unreacted precursors and by-products was discarded completely. The final product was either dried as a powder sample in a vacuum or dissolved in toluene or chloroform to form a stable sample solution.

Synthesis of $FeCr_2S_4$ NCs

The method for synthesis of $FeCr_2S_4$ NCs was similar to the previously described method except that the Se precursor was replaced by 1-DDT. 0.15 mmol (0.1 mL) of 1-DDT was injected into the mixture rapidly under vigorous stirring. The temperature was kept constant at 335 °C for 30 min. Then, the flask was cooled to room temperature. The purification process was as described previously. The final $FeCr_2S_4$ NCs were re-dispersed in toluene or chloroform to form a stable sample solution.

Device fabrication and characterization

A conductivity response device was fabricated (Fig. 5). An Au film with a thickness of 100 nm was constructed by radio frequency magnetron sputtering after a standard photolithography process. The middle section of the Au film was removed in order to deposit the concentrated colloidal NC solution through spin-coating, and then the prepared device was kept dry under vacuum conditions. The dried film was immersed in 0.2 mol L^{-1} EDT solution in anhydrous acetonitrile for 1 h and then dried by stable N_2 gas blowing. This process was repeated to increase the layer thickness, whereby any redundant organisms were removed by EDT treatment.

Electron imaging and elemental analysis were carried out using a high resolution transmission electron microscope (HRTEM, Hitachi-7600, Japan) at an acceleration voltage of 200 kV with a CCD camera (1350 × 1040), a scanning electron microscope (SEM, Hitachi-S4700, Japan) and an energy dispersive X-ray spectrometer (EDX). XRD analysis was carried out using an X-ray diffractometer (Empyrean series-2, Netherlands). Optical spectra were obtained using a UV-vis spectrophotometer (Scinco S310, Korea) and FT-IR spectrometer (Jasco 6300, Japan). Thermal gravimetric analysis (TGA, Scinco N-1000,

Korea) was carried out under a N_2 atmosphere at a heating rate of 15 °C min^{-1} from room temperature to 800 °C. *I–V* characteristics were recorded using an Iviumstat Electrochemical Interface (two-point method, Netherlands). The magnetic properties of each NC were characterized by using a superconducting quantum interference device (MPMS5, USA, with a sensitivity of 10^{-8} emu, a field range of −7 T to +7 T, and a temperature range of 1.7 K to 400 K).

Results and discussion

TEM images showed that the $FeCr_2Se_4$ NCs were formed with a predominantly quadrilateral shape and a tan average size of 63.4 ± 1.7 nm (Fig. 1A and B and the inset). In the HRTEM micrograph of an individual NC, the lattice fringes were distinct and the NCs showed good crystallization with a *d*-spacing of 0.3315 nm, corresponding to the (201) reflection of monoclinic $FeCr_2Se_4$ NCs (Fig. 1C). The TEM images of the other NCs also indicated excellent morphology and high crystallinity (see Fig. S1†). The angles between the planes, as measured from the selected area electron diffraction (SAED) obtained from Fig. 1D, were consistent with the expected value for these two planes in a crystal lattice. The iron-based ternary sulfur NCs ($FeCr_2S_4$) were composed of mostly spherical particles (Fig. 2). The average size of the individual particles along the (220) direction of the NCs was 13.6 ± 0.6 nm. The *d*-spacing was 0.3531 nm, corresponding to the (220) planes of the daubreelite phase $FeCr_2S_4$ NCs.

Fig. S2† shows a dramatic morphology transformation of the respective NCs during the growth process. The average elemental composition of the samples was determined by EDX, resulting in a Fe/Cr/Se ratio of 1 : 1.67 : 3.87 for $FeCr_2Se_4$, and a Fe/Cr/S ratio of 1 : 2.13 : 3.64 for $FeCr_2S_4$ NCs (see Fig. S3 and S4†). Fig. S5† presents typical TEM images of the final products prepared by simple control of the molar ratios of the Fe, Cr, Se, and S precursors used in various ways during the same synthesis process. It is observed that the crystal morphology or size distribution of the NCs is quite different although nanostructures were obtained in all cases. We are at present investigating the influence of the precursors' molar ratio in OLA on the morphology and size of the NCs.

Fig. 3A presents powder X-ray diffraction (PXRD) patterns corresponding to the monoclinic and daubreelite phases of $FeCr_2Se_4$ and $FeCr_2S_4$, respectively. The major diffraction peaks were indexed as (201), (002), (310), (311), (003), and (313) reflections of $FeCr_2Se_4$ (ICCD no. 65-4103). Similar statistics

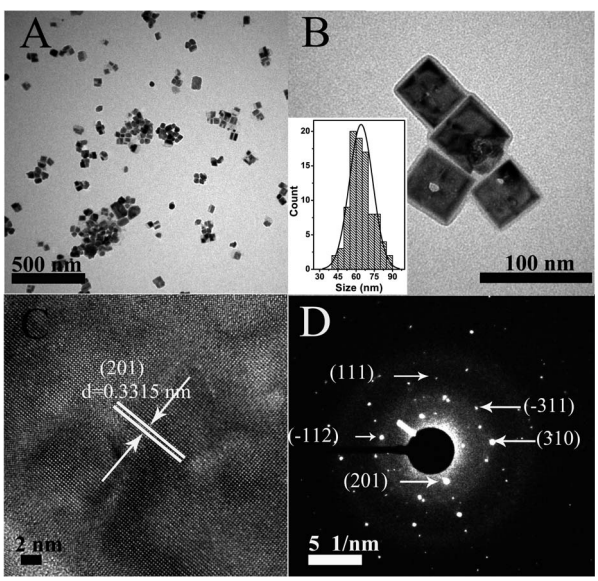

Fig. 1 (A and B) TEM images of $FeCr_2Se_4$ NCs, (C) HRTEM image of individual NCs, and (D) SAED pattern extracted from the image, (inset) size distribution of $FeCr_2Se_4$ NCs.

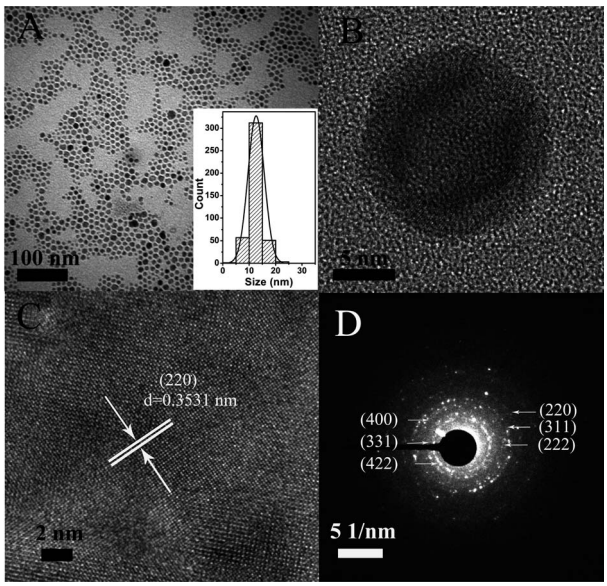

Fig. 2 (A) TEM image of $FeCr_2S_4$ NCs, (B and C) HR-TEM images of individual NCs, and (D) SAED pattern extracted from the image, (insets of A) size distribution of $FeCr_2S_4$ NCs.

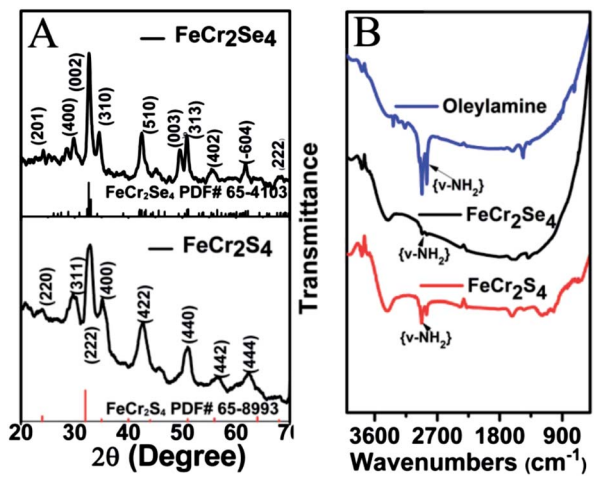

Fig. 3 (A) PXRD patterns of $FeCr_2Se_4$ (ICCD no. 65-4103) and $FeCr_2S_4$ (ICCD no. 65-8993) NCs and standard XRD patterns of parameters are shown at the bottom; (B) FT-IR spectra of $FeCr_2Se_4$ (up), $FeCr_2S_4$ NCs and oleylamine, respectively.

demonstrated the diffraction and reflections of $FeCr_2S_4$ NCs (ICCD no. 65-8993). In both cases the peaks correspond well to previously reported standard XRD patterns. In our novel crystal synthesis, OLA played multiple roles (*i.e.*, surfactant, solvent, and reducing agent) as it possesses a special molecular chain such as the double bond between the 9th and 10th carbon atoms. Restriction of rotation at the position of the double bond perhaps enables the elemental grains to attach together, thus reducing the surface energy.[13c] Therefore, NCs were passivated well and protected by OLA in our experiment.

This assumption of surface modification was confirmed by the FT-IR analysis of the characteristic peaks of OLA in the NCs (Fig. 3B). The absence of distinct IR peaks for the –SH group (2520 cm^{-1}) indicated that 1-DDT was not included in the final purified $FeCr_2S_4$ NCs, *i.e.*, the sulfur precursor was completely consumed in the reaction mixture. Moreover, the appearance of IR peaks for NH_2 groups (2975 cm^{-1}) can be explained by the formation of covalent bonds between the NH_2 group and the surface of each NC.

For the $FeCr_2Se_4$ and $FeCr_2S_4$ NCs, the color of the colloidal solution was brown-yellow and light-black, respectively. Absorption spectroscopy was subsequently performed to study the band gaps of these NCs. As shown in Fig. 4A, the onset absorption begins near 870 nm for $FeCr_2Se_4$ NCs and 854 nm for $FeCr_2S_4$ NCs. By calculating the band gaps of the NCs with the Kubelka–Munk method, the indirect band gaps of $FeCr_2Se_4$ NCs and $FeCr_2S_4$ NCs are determined to be 0.88 and 0.91 eV, respectively, and the direct band gaps are 2.36 eV for $FeCr_2Se_4$ NCs and 2.67 eV for $FeCr_2S_4$ NCs (Fig. 4B–D). These indirect band gaps are probably due to the size effect of the as-synthesized NCs or the change of the crystallographic structure of the NCs.[32]

The magnetizations of the two samples were measured as functions of the external magnetic field to evaluate the saturation magnetization at 5 K and 300 K (see Fig. S7†). The highest magnetization values obtained at 5 K for $FeCr_2Se_4$ and $FeCr_2S_4$ NCs are of a similar value of 0.2 emu g^{-1}. Both NCs exhibit magnetic behavior near room temperature whereas antiferromagnetic behavior with relatively low coercivity values of *ca.* 5×10^3 Oe ($FeCr_2Se_4$) and *ca.* 1×10^4 Oe ($FeCr_2S_4$) was observed at 5 K. The variation in magnetization as a function of temperature under field-cooled (FC) and zero-field-cooled (ZFC) conditions with an applied magnetic field of 50 Oe was analyzed. The observed blocking temperatures (T_b) from low-field 50 Oe measurements for $FeCr_2Se_4$ and $FeCr_2S_4$ NCs were 180 K and 176 K, respectively. The measurements showed a drop in the magnetization value to nearly zero at a temperature between 220 K and 230 K for both samples (see Fig. S8†). This can be ascribed to their Curie temperatures (T_c), which were somewhat higher than the bulk value of 180 K due to the orbital ordering transition at low temperatures due to a static cooperative Jahn–Teller effect.[29,32]

Fig. 5 shows *I–V* curves that indicate the conductivity of $FeCr_2Se_4$ and $FeCr_2S_4$ NCs in the devices. The SEM images of the device fabrication are presented in Fig. S9.† The current values from the films were obtained by adjusting the voltage from +4 V to −4 V, and the current values obtained were −3.25 μA to +3.25 μA ($FeCr_2Se_4$) and −2.33 μA to +2.33 μA ($FeCr_2S_4$), respectively. Furthermore, the two-point *I–V* plots showed a turn-on potential varying between −1.25 and +1.25 eV in the

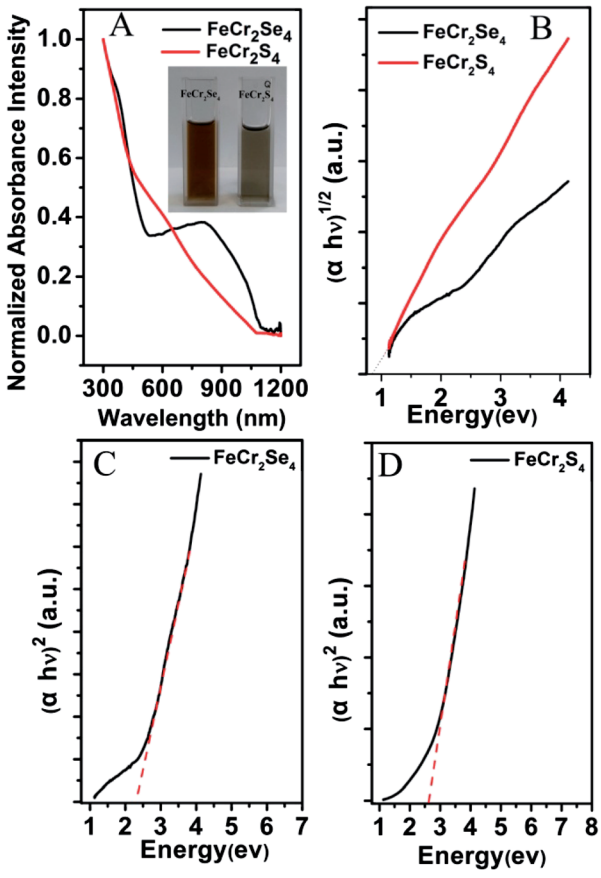

Fig. 4 (A) UV-visible absorption spectra of the $FeCr_2Se_4$ and $FeCr_2S_4$ NCs, (inset) digital photo of NC solution, left: $FeCr_2Se_4$, 6.55 mg L^{-1}; right: $FeCr_2S_4$, 7 mg L^{-1}. (B–D) Determination of band gaps by plotting $h\nu^{1/2}$ *vs.* energy for indirect band gaps (B), and $h\nu^2$ *vs.* energy for direct band gaps (C and D).

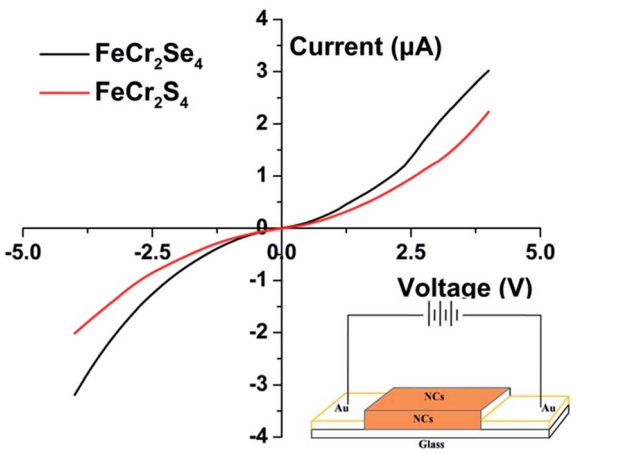

Fig. 5 *I–V* curves of drop-casting films constructed from NCs, black and red lines are current curves of $FeCr_2Se_4$ and $FeCr_2S_4$, respectively. (Inset) Configuration of conductivity measurements.

negative and positive quadrants, respectively (see Fig. S10†). Compared with similar experimental studies, the current value of these two kinds of NCs is similar to the values obtained from copper-based ternary or quaternary NCs employed in solar cell applications with 0.024 μA or 1.5 μA.[33,34] These iron-based ternary NCs are thus promising compounds as they are semiconducting and can be easily doped by substituting different chalcogens.[35] Additionally, the conductivity is usually dominated by photon or lattice conductivity, and the unit cell showed the ternary structures as monoclinic and daubreelite phases respectively.[36,37] It is natural that the crystalline size and lattice contribution affect internal structural distortions of the NC, resulting in the final conductivity. Among these two kinds of coordination structures in the NCs, Cr^{3+} has three electrons to fill the majority spin T_{2g} orbital (subsequent band) completely. Thus, Cr^{3+}may provide the metallic carriers. Furthermore, Fe^{2+} provides orbital electrons thus filling the orbital completely. So, these two kinds of NCs ($FeCr_2Se_4$ and $FeCr_2S_4$ NCs) can be considered as metal-like materials with high conductivity. Therefore, the conductive film maybe used as an efficient substrate in solar cell construction.

Conclusions

In summary, we have demonstrated a novel wet chemical synthesis method for iron-based ternary $FeCr_2Se_4$ and $FeCr_2S_4$ NCs. The method involved the hot injection of S and Se precursors into a boiling coordinating solvent containing the metal ions and surfactant molecules. The specific chemical compositions of these NCs combined with their precursors and initial electrical response show great potential for future electronic applications.

Acknowledgements

This research was supported by the Basic Science Research Program of the National Research Foundation of Korea (NRF) funded by the Ministry of Education (2013R1A1A4A010004637) and by the Civil & Military Technology Cooperation Program of the National Research Foundation of Korea (NRF) funded by the Ministry of Science, ICT & Future Planning (no. 2013M3C1A9055407).

Notes and references

1 (*a*) P. Feng, X. Bu and N. Zheng, *Acc. Chem. Res.*, 2005, **38**, 293; (*b*) I. Chung, J. I. Jang, C. D. Malliakas, J. B. Ketterson and M. G. Kanatzidis, *J. Am. Chem. Soc.*, 2009, **132**, 384.

2 (*a*) W. S. Sheldrick and M. Wachhold, *Angew. Chem., Int. Ed.*, 1997, **36**, 206; (*b*) M. Y. C. Teo, S. A. Kulinich, O. A. Plaksin and A. L. Zhu, *J. Phys. Chem. A*, 2010, **114**, 4173; (*c*) J. K. Sahoo, M. N. Tahir, A. Yella, T. D. Schladt, S. Pfeiffer, B. Nakhjavan, E. Mugnaioli, U. Kolb and W. Tremel, *Chem. Mater.*, 2011, **23**, 3534.

3 (*a*) M. Jr. Buchez, M. Moronne, P. Gin, S. Weiss and A. P. Alivisatos, *Science*, 1998, **281**, 2013; (*b*) L. A. Padilha, J. T. Stewart, R. L. Sandberg, W. K. Bae, W. K. Koh, J. M. Pietryga and V. I. Klimov, *Acc. Chem. Res.*, 2013, **46**, 1261.

4 Z. A. Peng and X. Peng, *J. Am. Chem. Soc.*, 2001, **123**, 183.

5 K. Ding, Z. Miao, Z. Liu, Z. Zhang, B. Han, G. An, S. Miao and Y. Xie, *J. Am. Chem. Soc.*, 2007, **129**, 6362.

6 A. Singh, H. Geaney, F. Laffir and K. M. Ryan, *J. Am. Chem. Soc.*, 2012, **134**, 2910.

7 R. B. Soriano, I. U. Arachchige, C. D. Malliakas, J. Wu and M. G. Kanatzidis, *J. Am. Chem. Soc.*, 2012, **135**, 768.

8 M. E. Norako and R. L. Brutchey, *Chem. Mater.*, 2010, **22**, 1613.

9 I. U. Arachchige, J. Wu, V. P. Dravid and M. G. Kanatzidis, *Adv. Mater.*, 2008, **20**, 3638.

10 M. Ibáñez, R. Zamani, W. Li, A. Shavel, J. Arbiol, J. R. Morante and A. Cabot, *Cryst. Growth Des.*, 2012, **12**, 1085.

11 C. Zou, L. Zhang, D. Lin, Y. Yang, Q. Li, X. Xu, X. Chen and S. Huang, *CrystEngComm*, 2011, **13**, 3310.

12 J. van Embden, K. Latham, N. W. Duffy and Y. Tachibana, *J. Am. Chem. Soc.*, 2013, **135**, 11562.

13 (*a*) J. Zwinscher and H. D. Lutz, *J. Solid State Chem.*, 1995, **118**, 43; (*b*) Y. H. Wang, N. Bao, L. Shen, P. Padhan and A. Gupta, *J. Am. Chem. Soc.*, 2007, **129**, 12408; (*c*) K. Ramasamy, D. Mazumdar, Z. Zhou, Y. H. Wang and A. Gupta, *J. Am. Chem. Soc.*, 2011, **133**, 20716.

14 M. E. Norako, M. J. Greaney and R. L. Brutchey, *J. Am. Chem. Soc.*, 2011, **134**, 23.

15 X. Lu, Z. Zhuang, Q. Peng and Y. Li, *CrystEngComm*, 2011, **13**, 4039.

16 (*a*) M. Kruszynska, H. Borchert, J. Parisi and J. Kolny-Olesiak, *J. Am. Chem. Soc.*, 2010, **132**, 15976; (*b*) S. Mourdikoudis and L. M. Liz-Marzan, *Chem. Mater.*, 2013, **25**, 1465.

17 M. R. Spender and A. H. Morrish, *Can. J. Phys.*, 1972, **50**, 1125.

18 M. A. Abosedira, *J. Mater. Sci.*, 2008, **8**, 660.

19 Y. Mizuguchi, F. Tomioka, S. Tsuda, T. Yamaguchi and Y. Takano, *Appl. Phys. Lett.*, 2008, **93**, 152505(03).

20 B. Yuan, W. Luan and S. T. Tu, *Dalton Trans.*, 2012, **41**, 772.

21 P. Kumar, S. Uma and R. Nagarajan, *Chem. Commun.*, 2013, **49**, 7316.

22 A. M. Wiltrout, N. J. Freymeyer, T. Machani, D. P. Rossi and K. E. Plass, *J. Mater. Chem.*, 2011, **21**, 19286.

23 S. Yoshimura, H. Asano, Y. Nakamura, K. Yamaji, Y. Takeda, M. Matsui, S. Ishida, Y. Nozaki and K. Matsuyama, *J. Appl. Phys.*, 2008, **103**, 7D716.

24 Y. Sun and J. A. Rogers, *Adv. Mater.*, 2007, **19**, 1897.

25 V. Zestrea, V. Y. Kodash, V. Felea, P. Petrenco, D. V. Quach, J. R. Groza and V. Tsurkan, *J. Mater. Sci.*, 2008, **43**, 660.

26 H. S. Carslaw and J. C. Jaeger, *Conduction of Heat in Solids*, 1959.

27 P. Gibart, M. Robbins and V. G. Lambrecht Jr, *J. Phys. Chem. Solids*, 1973, **34**, 1363.

28 B. I. Min, S. S. Baik, H. C. Choi, S. K. Kwon and J. S. Kang, *New J. Phys.*, 2008, **10**, 055014.

29 J. H. Kang, S. J. Kim, B. W. Lee and C. S. Kim, *J. Appl. Phys.*, 2006, **99**, 08F714.

30 S. J. Kim, B. S. Son, B. W. Lee and C. S. Kim, *J. Appl. Phys.*, 2004, **95**, 6837.
31 (*a*) J. Puthussery, S. Seefeld, N. Berry, M. Gibbs and M. Law, *J. Am. Chem. Soc.*, 2010, **133**, 716; (*b*) J. J. Wang, D. J. Xue, Y. G. Guo, J. S. Hu and L. J. Wan, *J. Am. Chem. Soc.*, 2011, **133**, 18558.
32 V. Tsurkan, O. Zaharko, F. Schrettle, C. Kant, J. Deisenhofer, H.-A. K. von Nidda, V. Felea, P. Lemmens, J. R. Groza and D. V. Quach, *Phys. Rev. B: Condens. Matter Mater. Phys.*, 2010, **81**, 184426.
33 Y. Liu, D. Yao, L. Shen, H. Zhang, X. Zhang and B. Yang, *J. Am. Chem. Soc.*, 2012, **134**, 7207.
34 J. Tang, S. Hinds, S. O. Kelley and E. H. Sargent, *Chem. Mater.*, 2008, **20**, 6906.
35 T. M. Adams, S. I. bdel-Khalik, S. M. Jeter and Z. H. Qureshi, *Int. J. Heat Mass Transfer*, 1998, **41**, 851.
36 G. J. Snyder, T. Caillat and J. P. Fleurial, *Phys. Rev. B: Condens. Matter Mater. Phys.*, 2000, **62**, 10185.
37 F. J. DiSalvo, *Science*, 1999, **285**, 703.